Title

Ruthenium Dye Excitations and Relaxations in Natural Sunlight

Journal

The Journal of Physical Chemistry A, 125(20)

ISSN

1089-5639

Authors

Cheshire, Thomas P

Houle, Frances A

Publication Date

2021-05-27

DOI

10.1021/acs.jpca.1c02386

Peer reviewed

111Equation Chapter 1 Section 1Ruthenium Dye Excitations and Relaxations in Natural Sunlight

Thomas P. Cheshire and Frances A. Houle*

Chemical Sciences Division, Lawrence Berkeley National Laboratory Berkeley, CA 94720

*Corresponding author: fahoule@lbl.gov

ABSTRACT: Solar harvesting devices using dyes convert the sun's energy to useable forms. The photophysics involved are generally investigated using time-resolved spectroscopic experiments with femtosecond to nanosecond resolution. We show that a kinetic framework constructed from transient and linear absorption measurements of metal-ligand charge transfer states for a set of ruthenium complexes in solution can be used to simulate the steady-state dynamics of dyes adsorbed on a substrate under diffuse solar radiation. Even though the intensity of sunlight is relatively low, double excitations to higher excited states can occur. The steady-state populations show that the dyes' triplet state is the main species present besides the ground state. While small, these persistent excited populations can influence reactivity over the extended periods of time that the systems operate. The results show that non-radiative and optical events (dye^{-1} s^{-1}) within the singlet manifold and from the triplet state exhibit a dependence on ligand substituents.

1. Introduction

Dyes used for solar energy conversion in the photoelectrodes of dye-sensitized solar cells (DSSC) and dye-sensitized photoelectrosynthesis cells (DSPEC) have been studied extensively with time-resolved spectroscopies,[1-3] providing important insights to their photophysical properties with intense, monochromatic light pump pulses.[4-5] Numerous kinetic models of ultrafast processes have been proposed for charge injection[6-8] and dye relaxation,[5, 9] and computational work has been performed to uncover the nature of molecular states and their transitions.[10-13] To our knowledge, how the data obtained under these experimental conditions relate to steady-state dye function under low intensity, continuous broad spectrum solar irradiation has not been evaluated, however. The populations of dye states at steady-state will influence how the chromophores interact with the surrounding electrolyte, catalysts, and their semiconductor substrate, as well as other chromophores when present at significant molar densities. It is essential to know what these populations are in order to evaluate the role the dyes play in full systems. The

kinetic detail introduced in the present study is central to a comprehensive reaction-diffusion framework for dye-sensitized systems that spans events from the femtosecond to second timescales, and the nanoscopic to the macroscopic lengthscales,[4, 14] designed to bridge products and photocurrents to detailed molecular events.

2. Model Development

To model dye photophysical processes in sunlight, we start with a predictive kinetic model for ultrafast molecular excitations and relaxations of a series of 6 ruthenium polypyridyl chromophores in solution[4] that simulates quantitatively time-resolved spectroscopic signals. The energy diagram in Figure 1 illustrates absorption and emission events between the dyes' singlet states (blue) and between triplet and ground states (rose), excited state absorption (ESA) events (orange), and non-radiative events (gray and black). Curved lines indicate optical transitions not accompanied by an electronic transition such as ground state bleach (GSB) and ESAs signals in transient absorption (TA) in which the probe pulse induces an electronic coherence with a higher energy state and decoherence induces the generation of the measured signal.

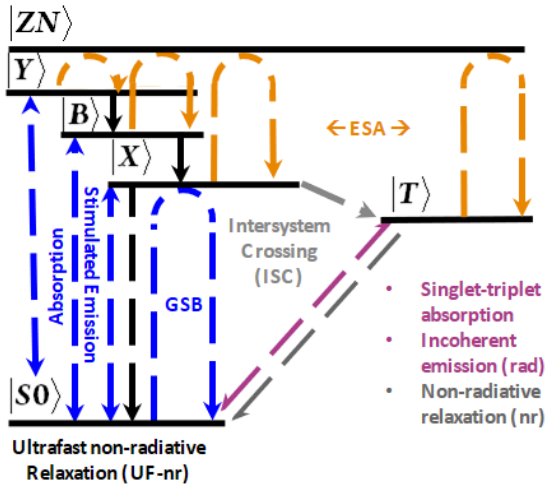

Figure 1. Jablonski diagram illustrating the optical and non-radiative transitions necessary for simulating the photophysics for set of 6 structurally related dyes, **6-Ru**. Transitions between the electronic ground state and the electronically excited singlet and triplet manifolds are represented in blue and rose, respectively. ESA are orange and non-radiative pathways are black or gray. **Model 0τ** (see text) was constructed to simulate transient measurements without intermediate state ¿B⟩. **Model 1τ(λ)** (see text) uses the entire scheme. This figure was adapted from Figure 8 in Ref [4].

2.1. Physical System Simulated

The chromophores (**Supporting Information (SI)** Section S1 Figure S1**)** are denoted as the set **6-Ru**: RuP, RuP2, RuP3, RuCP, RuCP2, and RuCP3. The kinetic model was developed from experimental linear absorption (LA) and TA data from 0.4 mM concentration of dyes in methanol[6] and time-resolved photoluminescence (TRPL) data from 0.15 mM concentration of dyes in aqueous 0.1 M $HClO_4$,[15] using the transitions involving the states ¿$S0$, ¿Y⟩, ¿X⟩, and ¿T⟩ shown in the scheme in Figure 1.

2.2. Simulations

The photophysical kinetics simulations were performed using the open access software Kinetiscope,[16] a stochastic kinetics simulator employing a core algorithm introduced by Bunker[17] and further developed by Gillespie[18] that tracks an ensemble of particles in event space rather than individual particles of an ensemble in physical space. Simulated GSB, excited state emission (ESE), and ESA signal components were in quantitative agreement with the experimentally measured change in absorption ΔA. We denote the model in Ref [4] as **Model 0τ** (**SI** Section S2 Table S1).

2.3. The Models

2.3.1. Model 0τ: Kinetic Model from Ultrafast Time-Resolved Data

RuP signal components for primary optical transitions and their wavelengths are shown in Figure 2 (the LA spectrum is in **SI** Section S3 Figure S2). Absorption component 1 at ~400 nm is associated with the excited singlet state ¿Y⟩, initially prepared by the TA pump pulse.[6] The peak of the metal-to-ligand charge transfer (MLCT) band, signal component 3, is identified as the peak of the GSB TA signal component, and is associated with absorption to state ¿X⟩. A low intensity broad absorption band centered at ~500 nm, signal component 4, is treated as direct absorption to the triplet manifold ¿T⟩. Five ESAs

(components 5-9) in the 500-700 nm regime are included in the kinetic framework, as well as incoherent emission from the triplet manifold. Non-radiative relaxations from relaxed singlet and triplet states return population back to the ground state. Additionally, **Model 0τ** encompasses a transition within the singlet manifold from the initially prepared state $¿Y⟩$ to a lower energy state $¿X⟩$ and intersystem crossing (ISC) from the singlet to triplet manifold. Relaxation of population from the lowest energy singlet state $¿X⟩$ to the ground state $¿S0⟩$ occurs on the femtosecond timescale and competes with ISC. Because **Model 0τ** was constructed to simulate time-resolved data, only these states and transitions were found to be crucial to yield agreement with TA and TRPL signal decays.

2.3.2. Model 0λ: Kinetic Model for Simulating Steady-State Data

Model 0λ is adapted from **Model 0τ** to simulate the steady-state response of continuous photoexcitation of dye adsorbed on a substrate that has a conduction band edge well above the lowest unoccupied molecular orbitals so that no charge injection occurs. Here, we assume that the perturbation of the photophysics on the picosecond timescale by the substrate is negligible. The TA pump-probe pulses used for **Model 0τ** are replaced with continuous broadband illumination. To simulate LA, **Model 0λ** assumes constant light irradiance of 1.85 W m^{-2} nm^{-1} across the 400-700 nm range, the relevant spectral region to natural light absorption for **6-Ru**. The initial ground state concentration, $2.5 \cdot 10^{16}$ molecules cm^{-2}, was estimated for dyes adsorbed to a mesoporous thin film from an absorbance measurement of Γ, where $\Gamma = A/\varepsilon$, A is the peak absorbance and ε is the extinction coefficient, and the reported adsorption equilibrium constants.[15] The pseudo-first order rate coefficients for each optical transition are calculated using the wavelength-dependent photon flux given in Equation Error: Reference source not found as the quotient of the irradiance $F(\lambda)$ and the energy $E(\lambda)$ within the spectral window $\Delta\lambda$. The steady-state populations for **6-Ru** are simulated from **Model 0λ** and the numbers of optical events at each wavelength are counted using marker species, discussed in **SI** Section S4.

$$\phi(\lambda)=\frac{F(\lambda)}{E(\lambda)\Delta\lambda} \qquad 22\backslash* \text{ MERGEFORMAT ()}$$

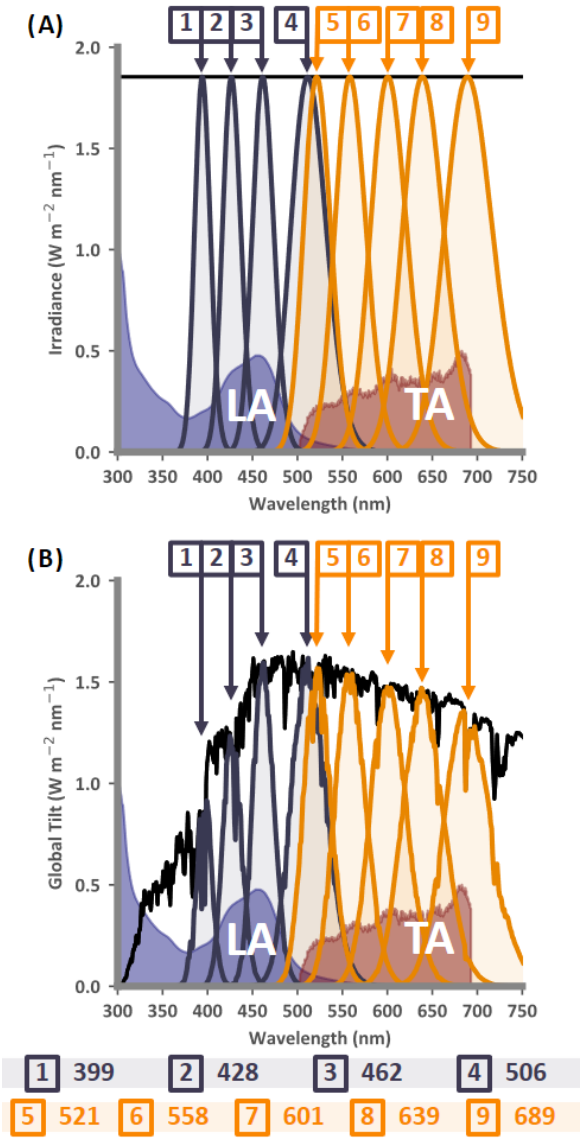

Figure 2. The product of the normalized signal components of the linear absorption (LA) and transient absorption (TA) spectra, and (A) constant irradiance and (B) the solar irradiance spectrum (AM 1.5 global tilt) representing the annual average intensities per wavelength in the United States (black lines).

As an initial validation of the steady-state model, we use those results with Equation Error: Reference source not found to compute LA spectra for all 6 dyes. LA measurements involve absorption to higher energy states, emission to lower energy states, and the non-radiative relaxations of excited states. It is generally assumed that only the linear signal is

measured, yet molecules that are promoted to excited states can undergo stimulated emission and have ESAs within the spectral range of the measurement. The absorption signal components A_i are the negative log of the simulated transmittance (i.e. the ratio of the transmitted photon flux to the incident photon flux), where n_{signal} are the total number of absorption events at that wavelength.

$$A_i = -\log_{10} \vee \frac{n_i - n_{Signal}}{n_i} \vee ¿ \qquad 33* \text{MERGEFORMAT ()}$$

In Figure 3 the experimental LA spectra (solid black) for set **6-Ru** are plotted together with simulated spectra using **Model 0λ** (dashed orange). It is evident that while the peak and red wing of the MLCT band are in good agreement with the experimental signals, a significant absorption at about 425 nm is not captured. Although **Model 0τ** reproduces the transient data well, **Model 0λ**—the corresponding version for steady-state, broadband excitation— does not generate accurate LA spectra. Constructing a kinetic framework from dynamic datasets for these dyes yields an incomplete picture of the molecular photophysics.

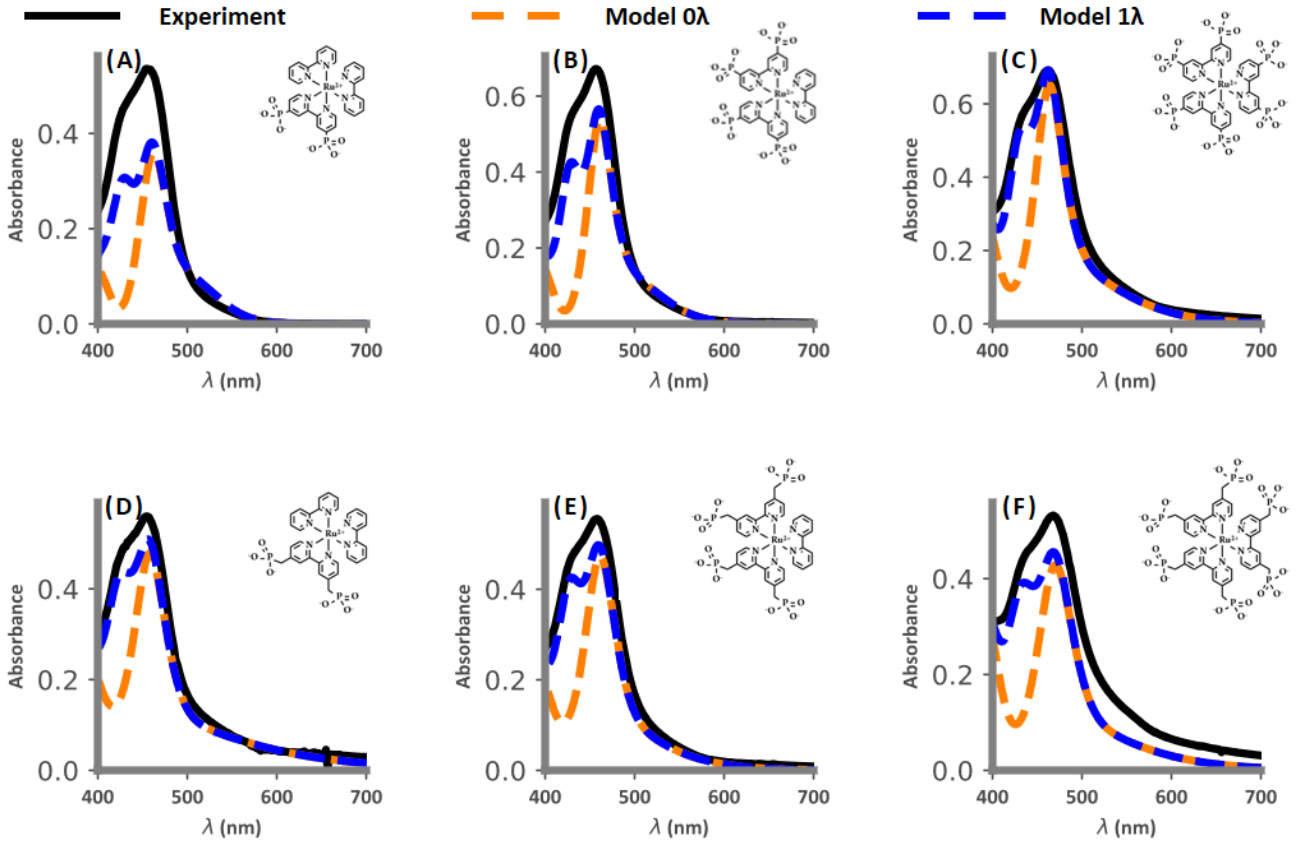

Figure 3. Experimental (solid black), simulated **Model 0λ** (dashed orange), and simulated **Model 1λ** (dashed blue) linear absorption spectra for the set of ruthenium complexes **6-Ru** in methanol: (A) RuP, (B) RuP2, (C) RuP3, (D) RuCP, (E) RuCP2, and (F) RuCP3.

2.3.3. Model 1λ: Improved Kinetic Model for Simulating Steady-State Data

To improve agreement with the LA spectra, we developed an extended framework, denoted **Model 1λ**, which includes a set of mechanistic steps for a state intermediate to the two singlet states in **Model 0λ.** The highest energy singlet state, the intermediate or "bridging" singlet state, and the relaxed singlet state, $¿Y⟩$, $¿B⟩$, and $¿X⟩$, are accessible to the ground state $¿S0⟩$ following photoexcitation from approximately 400 nm, 430 nm, and 460 nm light, respectively. To fully integrate $¿B⟩$ into our kinetic framework, transitions within the excited singlet manifold also need to be introduced; splitting the non-radiative transition from $¿Y⟩$ to $¿X⟩$ into two transitions from $¿Y⟩$ to $¿B⟩$ and $¿B⟩$ to

¿X⟩. The mechanistic steps associated with state ¿B⟩ extending **Model 0τ** to **Model 1λ** can be found in **SI** Section S5, Equations (S1)-(S7).

2.3.4. Model 1τ: Updated Kinetic Model for Simulating Time-Resolved Data

The addition of these transitions brings into close agreement the overall intensities and lineshapes of the simulated spectra using **Model 1λ** (dashed blue) in Figure 3 with the experimental signals. Specific wavelengths for each chromophore are reported in **SI** Section S6 Table S2. To ensure that the expanded model correctly predicts the transient signals as well, simulations using **Model 1τ** (dashed orange) are compared with simulated signals using **Model 0τ** (dashed blue) and the experimental signal (solid black) in Figure 4 (simulated ESAs in SI section S7.1 Figures S3-S7). The addition of the intermediate state ¿B⟩ does not have a significant effect on simulated intensities >1 ps, the difference in ΔA on the picosecond timescale between **Model 0τ** and **Model 1τ** is less than the variance in the experimental signal. On the femtosecond timescale, decay of the simulated GSB is generally steeper in **Model 1τ** because the larger rate coefficients for relaxation within the singlet manifold make it more competitive with stimulated emission than in **Model 0τ**. From the TA, both models are in quantitative agreement with experimental signals; however, the simulations of the LA spectra indicate that **Model 1τ(λ)** is the more complete framework. Analysis of pulsed excitations is insufficient for **6-Ru**: time-resolved and steady-state dynamics are both necessary to construct a comprehensive model of the dyes' photophysical responses. Rate coefficients are reported in full in **SI** Section S7 Table S3.

While kinetic analysis of experimental data is informative, there are limits to what can be learned. The simulated LA spectra are in poor agreement with experimental data without bridging state ¿B⟩. By including it, **Model 1λ** reproduces the LA signals of **6-Ru**, but the fundamental nature of ¿B⟩ and its non-radiative transitions cannot be conclusively determined. It is not obligatory to know the nature of the states and transitions included in

a kinetic framework, only that they are both necessary and sufficient to model the physics of interest. That this state had to be invoked points to a gap in knowledge about the photophysics of this important class of dyes. It is insufficient to validate a proposed kinetic model against a single set of conditions—**Model 0τ** and **Model 1τ** both simulate TA spectra in good agreement with time-resolved data. Tests for a model's uniqueness are also important and **Model 0λ** cannot reproduce the steady-state measurements.

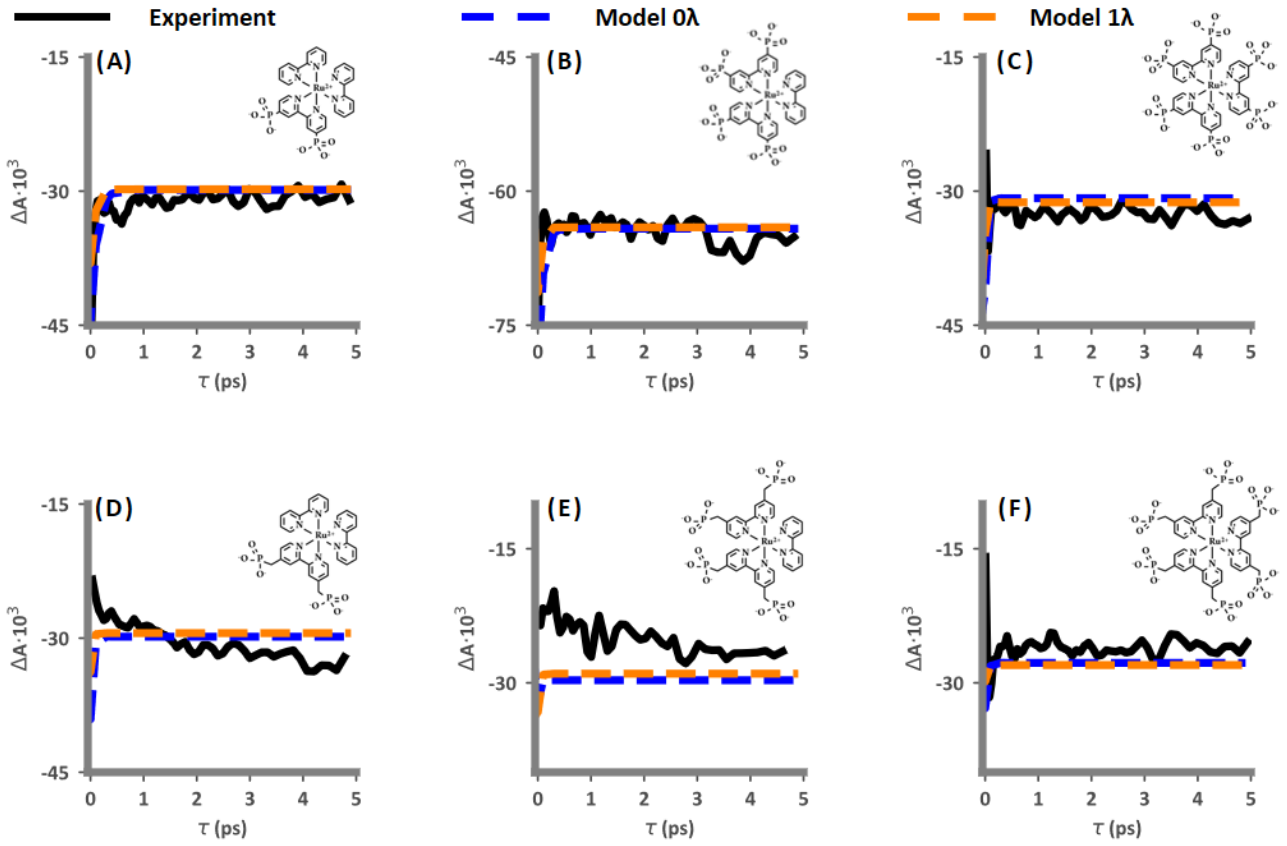

Figure 4. Transient absorption GSB signal decays for the set of ruthenium complexes **6-Ru** in methanol: (A) RuP, (B) RuP2, (C) RuP3, (D) RuCP, (E) RuCP2, and (F) RuCP3. Experimental (solid black), simulated from **Model 0τ** (dashed blue), and simulated from **Model 1τ** (dashed orange).

2.3.5. Model Sλ: Kinetic Model for Simulating Photoexcitations under 1-Sun Conditions

With the validated scheme for LA in hand, the solar irradiation spectrum[19-21] in Figure 2B (solid black) can be used to calculate dye populations under natural sunlight. The product

of the normalized signal components of the LA and TA spectra—fit as sums of Gaussians in ref [4]—and the AM 1.5 global tilt spectrum provide a foundation for capturing the response of set **6-Ru** under 1-sun conditions (details in **SI** Section S8). The optical rate coefficients are then given by Equation Error: Reference source not found:

$$k_{Solar:i,f} = k_{i,f} \cdot \int I_{Solar:i,f}(\lambda)\, d\lambda \,, \qquad 44\backslash* \text{ MERGEFORMAT ()}$$

where the wavelength-dependent solar intensity $I_{Solar:i,f}(\lambda)$ and the optical rate coefficients $k_{i,f}$ for transitions from initial state i to final state f are combined to yield the solar optical rate coefficients $k_{Solar:i,f}(\lambda)$. **Model Sλ** is the same framework as **Model 1λ**, with the optical rate coefficients replaced by the solar optical rate coefficients, **SI** Section S9 Table S4. The simulations, which use discrete rather than continuum methods, are run for 10 μs in simulation time, sufficient to reach steady-state populations, using 1:1 ratio of simulated particles to physical dyes. The assumed area is 1500 μm^2 and the initial number of dyes in the ground state is $\sim 3.6 \cdot 10^{11}$.

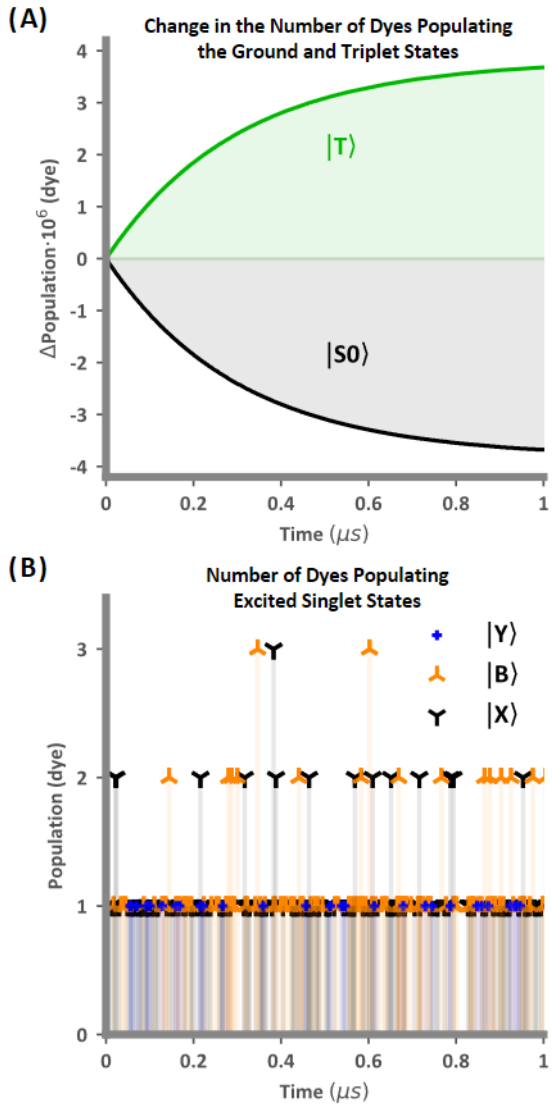

Figure 5. (A) Time-dependent ground state ¿$S0$⟩ and excited triplet ¿T⟩ state populations and (B) excited singlet state populations (¿Y⟩, ¿B⟩, and ¿X⟩) of the dye RuP from continuous illumination of a 1500 μm^2 region under 1-sun conditions. Steady-state in the simulations is reached in approximately 1 μs. The full data for 10 μs are shown in **SI** Section S10, Figures S9-S14.

3. Results and Discussion

Simulations using **Model Sλ** for set **6-Ru** yield steady-state data of populations and excitations in Figure 5 (**SI** Section S10, Figures S9-S14) and Figure 6, respectively. Figure 5A shows the change in the number of RuP dyes populating states ¿$S0$⟩ and ¿T⟩ within the 1500 μm^2 area used in the simulations. The number of populated states ¿Y⟩, ¿B⟩, and ¿X⟩ in the same region are exhibited in Figure 5B. It is noteable that the change in the

ground state populations is primarily reflected in the change of the triplet population, and the excited singlet populations remain relatively low.

The total numbers of specific transitions in 10 μs are tracked using the cumulative marker species tally for radiative and non-radiative events. Figure 6 shows—from left to right—the frequency of radiative (blue) and non-radiative (black) events per dye per second (dye^{-1} s^{-1}); the fraction of relaxation events within the excited singlet manifold (green), non-radiative relaxation events from the lowest energy singlet manifold (orange), and non-radiative relaxation events from the triplet manifold (gray) relative to the total number of non-radiative events; and the number of ESA (outer circle) and ESE (inner circle) events per million (epm) total events. Reproducibility error is negligibly small and not exhibited in panels (A) and (C) (see **SI** Section S11 Table S5).

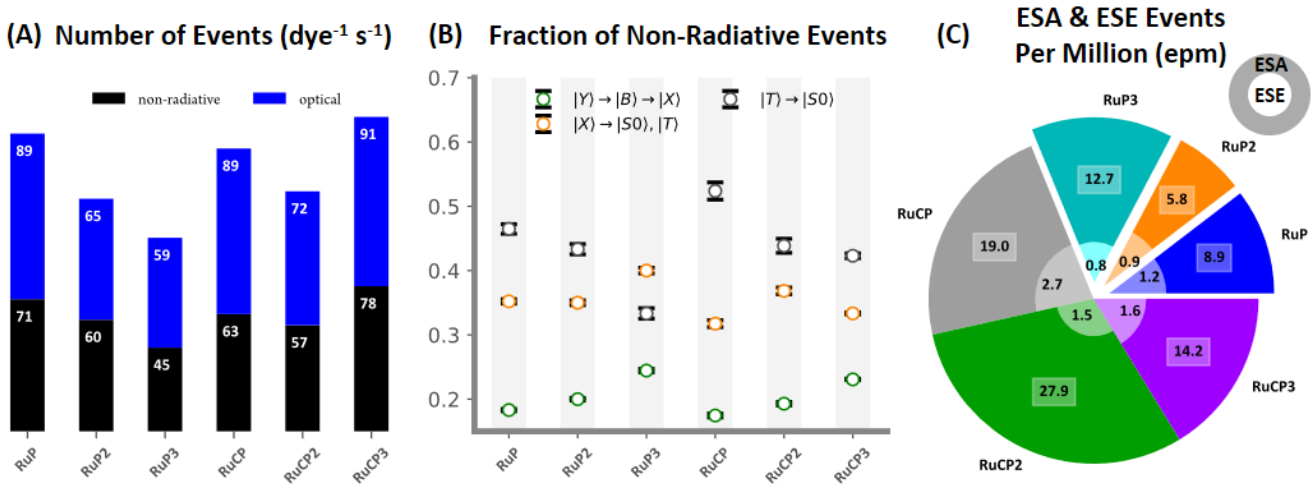

Figure 6. (A) Frequency of non-radiative (black) and optical (blue) events per dye, (B) fraction of non-radiative relaxation events within the excited singlet manifold (green), from the lowest energy singlet state (orange), and from the triplet manifold (gray) to total non-radiative events, and (C) and excited state absorption (ESA) and excited state emission (ESE) events per million (epm) total events for the set of dyes **6-Ru**.

The frequency of optical events is primarily governed by the solar optical rate coefficients for absorption: overlap with the solar spectrum (i.e. AM 1.5 global tilt), peak intensity, and linewidth of the signal components. The frequency of events—the sum of non-radiative (black) and optical events (blue) in Figure 6A—ranges from approximately

100-200 dye^{-1} s^{-1}, showing important trends with dye structure. The frequency decreases as the number of phosphonated or methyl-phosphonated bipyridine ligands decreases, with the exception of RuCP3. The trend is the same for optical (approximately 50-60% of total events) and non-radiative (approximately 40-50% of total events) transitions when considering them independently.

There are notable trends discernable in Figure 6B, the fraction of total non-radiative transitions. The proportion of transitions from the triplet and singlet manifolds are comparable, showing they have similar rates even though the rate coefficients for non-radiative relaxation from singlet states are ~10^{13} s^{-1} and from triplet states are ~10^{6} s^{-1}. This is because the population in the triplet manifolds of the dyes are more than six orders of magnitude greater than in the singlet manifolds. Despite having similar rates, the fractions of transitions leaving the triplet state, leaving the excited singlet manifold, and relaxing within the excited singlet manifold decrease in that order. The greater fraction of non-radiative transitions from the triplet manifold than to the triplet manifold indicates that much of the triplet population is from direct absorption, rather than from an excited state spin transition.

Also observed in Figure 6B, as the number of phosphonated or methyl-phosphonated bipyridine ligands increase, the fraction of relaxation events within the singlet manifold and from the singlet manifold increases—with the exception of relaxation events from the RuCP3 singlet manifold—and the proportion of relaxation events from the triplet state decreases. The origin of the correlation between fractions of non-radiative events and numbers of phosphonate ligands is not revealed in this work. Previous studies have reported correlations of lifetimes with the reorganization energy for the phosphonate-bipyridine stretch[6] and the total reorganization energy,[8] which may be relevant. Such dynamics would be folded into the rate coefficients extracted from our previous studies.[4]

The optical transitions for all chromophores are dominated by absorption from the ground state and the GSB signal components. ESA and ESE are very rare optical events, as is incoherent emission (Figure 6A and Figure 6C), however they do occur even under diffuse illumination because there is enough triplet population to make the probabilities of interactions non-negligible. The solar excitation rate coefficients are on the order of 10^0-10^1 s^{-1} and steady state dye populations in the ground state, triplet manifold, and excited singlet states are on the order of 10^{11}, 10^6, and 10^0 respectively. It is significant to note that, though reactions following a single absorption event are more probable than reactions involving multiple absorption events, the simulated frequency of ESA events suggest photochemistry involving higher energy states is possible under natural illumination. There is considerable evidence that a persistent **6-Ru** triplet population can strongly influence the reactivity of a dye-sensitized system by generating $^1O_2$, a potent oxidizer and free radical chain reaction initiator, from dissolved oxygen.[22-26] That such channels for unwanted chemistry could be present in dye-sensitized systems for energy conversion must be considered.

It is tempting to compare these dye excitation frequencies and excited state populations to estimated electron injection frequencies from the literature for Ru-based dyes, which is important to understand device performance. At this point we have not established the charge injection kinetics, which may significantly influence the dye populations. Once in hand, it will be possible to use the full photophysical scheme to predict the overall injection frequencies and timing.

Lastly, in a previous study, we computed using Equation Error: Reference source not found ISC efficiencies, ϕ_{ISC}<1, [4] less than reported in the literature.[27] The experimental TA GSB signals, seen here in Figure 4, were not reproducible without an ultrafast decay from the lowest energy state ¿X⟩ to the ground state ¿$S0$⟩. Using **Model Sλ**, a value more

directly comparable to the efficiency of excited states relaxing to a luminescing state, ϕ' as given by Ref [27], can be computed from Equation:

$$\phi_{ISC} = \frac{k_{ISC}}{k_{ISC} + k_{ufnr}} \quad 55\backslash* \text{ MERGEFORMAT ()}$$

$$\phi' = \frac{f_E}{Q - 1 + f_E} \quad 66\backslash* \text{ MERGEFORMAT ()}$$

such that f_E is the fraction of incident photons absorbed to directly populated the emitting state and Q is the ratio of relative luminescence yields from lower and higher energy states respectively. Integration of the Gaussian-like feature 4 in Figure 2B over spectral region of the FWHM and integrating over the same limits of the solar spectrum, we can estimate f_E. Q is calculated from the number of absorption events directly to the state ¿T⟩ and the number of excited states that enter ¿T⟩ from the singlet manifold. Values for f_E and Q were estimated for RuBPY in Ref [27] to be 0.9 and 1.01, respectively. Our results, shown in Table 1, for f_E agree well with this approximation, yet we compute Q to be more than 10% greater. RuP2 has more population transitioning from the singlet manifold to state ¿T⟩ than direct absorption in our simulations, making the computed ϕ' > 1, and therefore a meaningless result. Our calculation of ϕ' using the number of events is greater than the previously computed ϕ_{ISC} though still significantly less than unity.[4] Despite this difference, the photoluminescence (PL) efficiencies (quantum yield), $\phi_{PL}(\Phi_{PL})$, from Equation Error: Reference source not found (Equation Error: Reference source not found) are in good agreement with experimental observations.[15]

$$\phi_{PL} = \frac{n_{emission}}{n_{emission} + n_{non-radiative}} \quad 77\backslash* \text{ MERGEFORMAT ()}$$

$$\Phi_{PL} = \frac{n_{emission}}{n_{absorption}} \quad 88\backslash* \text{ MERGEFORMAT ()}$$

Table 1. Values related to the efficiency of ISC

	F_E	Q	ϕ'	ϕ_{ISC}[a]	$\phi_{PL,\sim¿(\Phi_{PL})¿}$[b]	ϕ_{PL}[c]
RuP	0.85	1.2	0.82	0.63 (0.64)	0.033 (0.025)	0.033
RuP2	—	—	—	0.80 (0.81)	0.036 (0.030)	0.036
RuP3	0.90	1.8	0.52	0.33 (0.33)	0.053 (0.028)	0.052
RuCP	0.84	2.3	0.40	0.56 (0.55)	0.050 (0.039)	0.050
RuCP2	0.78	1.3	0.76	0.56 (0.57)	0.050 (0.035)	0.046
RuCP3	0.92	1.1	0.89	0.64 (0.64)	0.043 (0.033)	0.041

[a] Values from Ref [4] (computed from steady-state simulations using number of ISC and ultrafast non-radiative transitions in place of rate coefficients in Equation Error: Reference source not found.

[b] Values computed from Equation Error: Reference source not found (Equation Error: Reference source not found).

[c] Ref [15]

4. Conclusions

In this work we show that the ultrafast photophysics of dyes used in DSSC and DSPEC devices together with their linear spectroscopy can be used to predict the steady-state excitations of dyes adsorbed on substrates and illuminated by natural sunlight. Radiative and non-radiative relaxations occur with approximately equal frequency. Analysis of our simulations has uncovered a relation between dye structure and the frequency of absorption and relaxation events under diffuse solar illumination, including rare events such as ESA and ESE that occur at the ppm-level, which was not accessible in our previous analysis of transient measurements.[4] Increasing the numbers of phosphonated ligands increases the frequency of relaxations within the singlet manifold, and decreases relaxations from the triplet state to the ground state. The influence of the ligands on intersystem crossing is not large. In the absence of charge injection, excited states have the potential to influence reactivity with surrounding chemical species. Although the populations of excited singlets and triplets are small, their impacts could be felt over the extended time periods of hours to days that dye-sensitized systems operate if they can

instigate chemical chain or cascading reactions. How these populations evolve when charge injection can occur is currently under investigation.

Acknowledgments

This material is based upon work supported by the U.S. Department of Energy, Office of Science, Office of Basic Energy Sciences, Chemical Sciences, Geosciences, and Biosciences Division, in the Solar Photochemistry Program under Contract No. DE-AC02-05CH11231.

Supporting Information. The chromophores in set **6-Ru**, linear absorption spectrum for dye RuP between 300 nm and 600 nm, **Model 0τ(λ)**, **Model 1τ(λ)**, **Model Sλ**, simulated ESA spectra, population data, and reproducibility.

REFERENCES

1. Brown, A. M.; McCusker, C. E.; Carey, M. C.; Blanco-Rodriguez, A. M.; Towrie, M.; Clark, I. P.; Vlcek, A.; McCusker, J. K., Vibrational Relaxation and Redistribution Dynamics in Ruthenium(Ii) Polypyridyl-Based Charge-Transfer Excited States: A Combined Ultrafast Electronic and Infrared Absorption Study. *J Phys Chem A* **2018**, *122*, 7941-7953.
2. Cannizzo, A.; van Mourik, F.; Gawelda, W.; Zgrablic, G.; Bressler, C.; Chergui, M., Broadband Femtosecond Fluorescence Spectroscopy of [Ru(Bpy)3]2+. *Angew Chem Int Ed Engl* **2006**, *45*, 3174-6.
3. Yoon, S.; Kukura, P.; Stuart, C. M.; Mathies, R. A., Direct Observation of the Ultrafast Intersystem Crossing in Tris(2,2′-Bipyridine)Ruthenium(Ii) Using Femtosecond Stimulated Raman Spectroscopy. *Molecular Physics* **2006**, *104*, 1275-1282.
4. Cheshire, T. P.; Brennaman, M. K.; Giokas, P. G.; Zigler, D. F.; Moran, A. M.; Papanikolas, J. M.; Meyer, G. J.; Meyer, T. J.; Houle, F. A., Ultrafast Relaxations in Ruthenium Polypyridyl Chromophores Determined by Stochastic Kinetics Simulations. *J Phys Chem B* **2020**, *124*, 5971-5985.
5. Dongare, P.; Myron, B. D. B.; Wang, L.; Thompson, D. W.; Meyer, T. J., [Ru(Bpy)3]2+∗ Revisited. Is It Localized or Delocalized? How Does It Decay? *Coordin Chem Rev* **2017**, *345*, 86-107.
6. Giokas, P. G.; Miller, S. A.; Hanson, K.; Norris, M. R.; Glasson, C. R. K.; Concepcion, J. J.; Bettis, S. E.; Meyer, T. J.; Moran, A. M., Spectroscopy and Dynamics of Phosphonate-Derivatized Ruthenium Complexes on Tio2. *J Phys Chem C* **2013**, *117*, 812-824.
7. Swierk, J. R.; McCool, N. S.; Nemes, C. T.; Mallouk, T. E.; Schmuttenmaer, C. A., Ultrafast Electron Injection Dynamics of Photoanodes for Water-Splitting Dye-Sensitized Photoelectrochemical Cells. *The Journal of Physical Chemistry C* **2016**, *120*, 5940-5948.
8. Zigler, D. F., et al., Disentangling the Physical Processes Responsible for the Kinetic Complexity in Interfacial Electron Transfer of Excited Ru(Ii) Polypyridyl Dyes on Tio2. *J Am Chem Soc* **2016**, *138*, 4426-38.
9. Thompson, D. W.; Ito, A.; Meyer, T. J., [Ru(Bpy)3]2+* and Other Remarkable Metal-to-Ligand Charge Transfer (Mlct) Excited States. *Pure Appl Chem* **2013**, *85*, 1257-1305.
10. Daul, C.; Baerends, E. J.; Vernooijs, P., A Density-Functional Study of the Mlct States of [Ru(Bpy)3]2+ in D3 Symmetry. *Inorg Chem* **1994**, *33*, 3538-3543.
11. Kober, E. M.; Caspar, J. V.; Lumpkin, R. S.; Meyer, T. J., Application of the Energy-Gap Law to Excited-State Decay of Osmium(Ii) Polypyridine Complexes - Calculation of Relative Nonradiative Decay-Rates from Emission Spectral Profiles. *J Phys Chem-Us* **1986**, *90*, 3722-3734.
12. Kober, E. M.; Meyer, T. J., Concerning the Absorption Spectra of the Ions M(Bpy)32+ (M = Fe, Ru, Os; Bpy = 2,2'-Bipyridine). *Inorg Chem* **1982**, *21*, 3967-3977.
13. Ronca, E.; De Angelis, F.; Fantacci, S., Time-Dependent Density Functional Theory Modeling of Spin–Orbit Coupling in Ruthenium and Osmium Solar Cell Sensitizers. *The Journal of Physical Chemistry C* **2014**, *118*, 17067-17078.

14. Houle, F. A., Reaction–Transport Coupling in a Nanostructured Porous Electrode. *The Journal of Physical Chemistry C* **2019**, *123*, 14459-14467.
15. Hanson, K., et al., Structure–Property Relationships in Phosphonate-Derivatized, Ruii Polypyridyl Dyes on Metal Oxide Surfaces in an Aqueous Environment. *J. Phys. Chem. C* **2012**, *116*, 14837-14847.
16. Hinsberg, W. D.; Houle, F. A.; Sanchez, M. I.; Wallraff, G. M., Chemical and Physical Aspects of the Post-Exposure Baking Process Used for Positive-Tone Chemically Amplified Resists. *Ibm J Res Dev* **2001**, *45*, 667-682.
17. Bunker, D. L.; Garrett, B.; Kleindienst, T.; Long, G. S., Discrete Simulation Methods in Combustion Kinetics. *Combust. Flame* **1974**, *23*, 373-379.
18. Gillespie, D. T., A General Method for Numerically Simulating the Stochastic Time Evolution of Coupled Chemical Reactions. *Journal of Computational Physics* **1976**, *22*, 403-434.
19. Gueymard, C. A., Parameterized Transmittance Model for Direct Beam and Circumsolar Spectral Irradiance. *Sol Energy* **2001**, *71*, 325-346.
20. Gueymard, C. A., The Sun's Total and Spectral Irradiance for Solar Energy Applications and Solar Radiation Models. *Sol Energy* **2004**, *76*, 423-453.
21. Gueymard, C. A.; Myers, D.; Emery, K., Proposed Reference Irradiance Spectra for Solar Energy Systems Testing. *Sol Energy* **2002**, *73*, 443-467.
22. Demas, J. N.; Adamson, A. W., New Photosensitizer - Tris(2,2'-Bipyridine)Ruthenium(Ii) Chloride. *Journal of the American Chemical Society* **1971**, *93*, 1800-&.
23. Navon, G.; Sutin, N., Mechanism of the Quenching of the Phosphorescence of Tris(2,2'-Bipyridine)Ruthenium(Ii) by Some Cobalt(Iii) and Ruthenium(Iii) Complexes. *Inorg Chem* **2002**, *13*, 2159-2164.
24. Omar Zahir, K.; Haim, A., Yields of Singlet Dioxygen Produced by the Reaction between the Excited State of Tris(Bipyridine)Ruthenium(Ii) and Triplet Dioxygen in Various Solvents. *Journal of Photochemistry and Photobiology A: Chemistry* **1992**, *63*, 167-172.
25. Kohler, L.; Nease, L.; Vo, P.; Garofolo, J.; Heidary, D. K.; Thummel, R. P.; Glazer, E. C., Photochemical and Photobiological Activity of Ru(Ii) Homoleptic and Heteroleptic Complexes Containing Methylated Bipyridyl-Type Ligands. *Inorg Chem* **2017**, *56*, 12214-12223.
26. Wang, J.-L.; Wang, C.; deKrafft, K. E.; Lin, W., Cross-Linked Polymers with Exceptionally High Ru(Bipy)32+ Loadings for Efficient Heterogeneous Photocatalysis. *ACS Catalysis* **2012**, *2*, 417-424.
27. Demas, J. N.; Taylor, D. G., On the "Intersystem Crossing" Yields in Ruthenium(Ii) and Osmium(Ii) Photosensitizers. *Inorg Chem* **1979**, *18*, 3177-3179.

TOC Graphic